Ordering of iron vacancies in monoclinic jarosites

NICOLA V.Y. SCARLETT, IAN E. GREY,* AND HELEN E.A. BRAND

CSIRO Division of Process Science and Engineering, Box 312, Clayton South, Victoria 3169, Australia

ABSTRACT

The results of in situ synchrotron X-ray powder diffraction experiments conducted during the synthesis of iron-deficient Na^+/H_3O^+ and K^+/H_3O^+ jarosites at temperatures in the range 80 to 120 °C are presented. They demonstrate that samples can be prepared in which the iron-site vacancies are ordered. The ordering is accompanied by a lowering of symmetry, from rhombohedral, space group $R\bar{3}m$, to monoclinic, $C2/m$. The implications for magnetic properties are discussed.

Keywords: Jarosites, iron-deficient jarosites, monoclinic jarosites, iron-site vacancy ordering in jarosites

INTRODUCTION

Jarosite group minerals, $AFe_3(SO_4)_2(OH)_6$, where A = large cations such as K^+, Na^+, H_3O^+, play important roles in the environment, in metallurgical processes, and as industrial materials (Jones et al. 2006; Dutrizac and Jambor 2000; Kolitsch and Pring 2001). A recent resurgence in research on jarosite has been inspired by its identification as a possible hydrated mineral on Mars, using Mössbauer spectroscopy (Klingelhöfer et al. 2004; Papike et al. 2006). Jarosites are also of considerable theoretical interest as model compounds for spin frustration in kagomé-Heisenberg antiferromagnetic materials (Wills et al. 2000; Grohol et al. 2003). Previous studies on the synthesis of jarosites have shown that the compositions depend strongly on the preparative conditions (Dutrizac 1983). Elevated temperatures and pressures in hydrothermal preparations and high iron concentration in solution favor stoichiometric phases, whereas temperatures closer to ambient (<100 °C) result in high concentrations of hydronium ions in the A position and in iron deficiencies. Most studies on both natural and synthetic jarosites report the symmetry to be rhombohedral, space group $R\bar{3}m$, with hexagonal cell parameters $a_h \sim 7.3$ Å, $c_h \sim 17$ Å, although one laboratory has reported monoclinic symmetry for synthetic K-jarosite (Göttlicher et al. 2000).

Synthetic jarosites commonly have iron site deficiencies, which cause inconsistencies in the measured magnetic properties (Frunzke et al. 2001; Wills et al. 2000), but the structural nature and influence of iron non-stoichiometry is not well understood. We report here the results of in situ synchrotron powder X-ray diffraction (PXRD) experiments on the synthesis of iron-deficient jarosites that demonstrate that samples can be prepared in which the iron-site vacancies are ordered. The ordering is accompanied by a lowering of symmetry, from rhombohedral, $R\bar{3}m$, to monoclinic, $C2/m$. The implications for magnetic properties are discussed.

EXPERIMENTAL METHODS

This study focused on jarosites with A = K^+/H_3O^+ and Na^+/H_3O^+, which are referred to here as K-jarosite and Na-jarosite, respectively. 1.74 g of $Fe_2(SO_4)_3 \cdot 11H_2O$

and 0.57 g of Na_2SO_4, or 0.23/0.46/0.70 g of K_2SO_4 were dissolved in 10 mL of deionized water and filtered through a Millipore syringe filter to remove any undissolved particles. Portions of each solution were transferred to 1.0 mm quartz capillaries for synchrotron PXRD experiments. Data sets at temperatures of 80, 95, and 120 °C were collected on the powder diffraction beamline at the Australian Synchrotron, using a wavelength of 0.9523 Å. The capillaries were pressurized using nitrogen gas at 4 bar to prevent boiling of the solution and heated with a hot air blower using equipment previously described (Madsen et al. 2005). Data sets were collected every 60 s during the synthesis experiments, for periods of 2 to 5 h, while the capillary was oscillated about its axis. At the end of the experiment, a 180 s data set was collected and used in a Rietveld refinement, to establish profile parameters, atomic coordinates, and isotropic displacement parameters for the product. The profile parameters included provision for modeling sample displacement effects due to diffraction from sample crystals on opposing sides of the 1 mm diameter capillary. The TOPAS software was used for the Rietveld refinements (Bruker 2008). Starting atomic coordinates for the refinement of the 180 s data set, in space group $C2/m$, were generated from published coordinates for rhombohedral Na-jarosite (Basciano and Peterson 2008), transformed to the monoclinic cell. The refined coordinates, atomic displacement, and sample displacement parameters were then fixed for Rietveld refinements of the 200 or so 60 s data sets, in which the scale, unit-cell parameters, and site occupancies for Fe and Na/K sites were the key refinement parameters.

Larger scale syntheses using the same molar ratios as for the synchrotron experiments were conducted in sealed polytetrafluoroethylene containers to obtain enough material for chemical analyses. Samples were analyzed for Na/K, Fe, and S by ICP-OES after dissolution in 1:1 nitric acid. Water content was measured by thermogravimetric analysis.

RESULTS AND DISCUSSION

The high resolution obtained in the synchrotron PXRD patterns enabled observation of peak splitting due to a lowering of symmetry. This is illustrated in Figure 1, showing part of the Rietveld-fitted PXRD patterns for Na-jarosite and K-jarosite prepared at 95 °C. The pattern for the K-jarosite conforms to rhombohedral symmetry, whereas peak splitting occurs for the Na-jarosite. The lack of splitting of the $(009)_h$ (hexagonal indices) reflection and splitting of the peaks such as $(033)_h$ and $(027)_h$ into two peaks with an intensity ratio of 1:2 is characteristic of monoclinic symmetry. The small secondary splitting of the peaks (indicated by vertical arrows in Fig. 1, $\Delta2\theta = 0.03°$) is a sample displacement effect due to the sample offset between crystallites nucleating on opposing walls of the capillary. This observation attests to the high resolution obtained in the synchrotron experiments. The displacement splitting is not evident in the pattern of
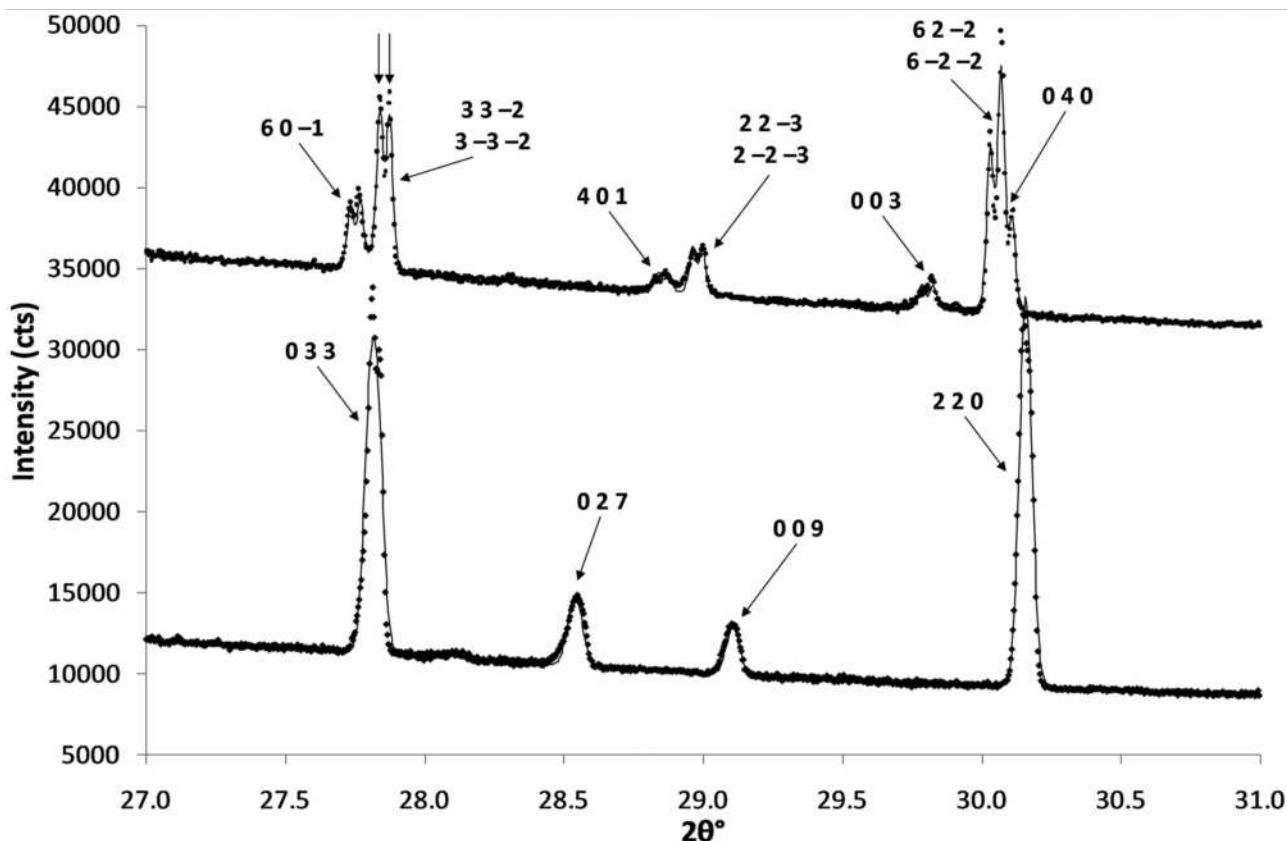
* E-mail: ian.grey@csiro.au

FIGURE 1. Part of Rietveld-fitted, 180 s synchrotron diffraction patterns for K-jarosite (lower) and Na-jarosite (upper, offset for clarity) prepared at 95 °C. Symbols are experimental points and lines correspond to the calculated patterns. The K-jarosite peaks are labeled with hexagonal indices, while the Na-jarosite peaks are labeled with monoclinic indices. An example of the secondary peak splitting due to sample displacement across the capillary is indicated by the vertical arrows.

the K-jarosite because the crystals formed more rapidly throughout the capillary volume. The sharpness of the (00l) reflections indicates that the synthesized samples do not contain a range of compositions (Basciano and Peterson 2007).

The clearest manifestation of the monoclinic distortion was obtained for Na-jarosite preparations (molar ratio [Fe]/[Na] = 1 in starting solution) heated at 80 and 95 °C. In contrast, K-jarosite with [Fe]/[K] = 1 in the starting solution did not show monoclinic splitting at 80 and 95 °C. Increasing the [Fe]/[K] ratio in the starting solution to 1.5 and then to 3 gave progressive evolution of low-angle shoulders in the XRD patterns due to a contribution from a monoclinic phase. At a synthesis temperature of 120 °C, the PXRD patterns for all samples showed broadening of the (00l) reflections, indicating a spread of compositions. Rietveld refinements of these patterns gave good fits for mixtures of rhombohedral and monoclinic jarosites. This preliminary report concentrates on results for the monoclinic Na-jarosite prepared at 95 °C. Analysis gave in wt% 47.3 Fe_2O_3, 4.85 Na_2O, 33.5 SO_3, and 14.2 H_2O. The calculated composition is $Na_{0.75}(H_3O)_{0.25}Fe_{2.84}$ $(SO_4)_2OH_{5.52}(H_2O)_{0.48}$.

The peaks in the pattern for Na-jarosite were fitted with a structural model based on a C-centered monoclinic cell, space group $C2/m$. The monoclinic cell is related to the hexagonal cell by the transformation matrix (1$\bar{1}$0, 110, $\frac{1}{3}\frac{1}{3}\frac{1}{3}$). The Rietveld refinement results are reported in Table 1. There are two independent iron atom sites in the $C2/m$ model, Fe1 at 0,0,½ and Fe2

at ¾,¼,½, shown in Figure 2. A striking result from the refinement of the PXRD data is the preferential ordering of vacancies into the Fe1 site. This is illustrated in Figure 3a, which shows refined site occupancy values from 50 min into the reaction until the completion of the experiment. The induction period for the onset of a precipitate in this experiment was about 40 min. Refined values from data between 40 and 50 min are considered to be unreliable because the diffracted peaks are barely observable above background. The occupancies of both Fe sites are initially equal, at ~0.92, corresponding to a random distribution of vacancies. With increasing time the occupancy of the Fe1 site decreases, while that of the Fe2 site increases, and reaches full occupancy after ~120 min. The occupancy of the Fe1 site reaches a minimum of ~0.83 after 150 min of reaction time at 95 °C. The

TABLE 1. Rietveld refinement results for Na-jarosite synthesized in situ at the Australian Synchrotron at 95 °C

Atom	x	y	z	B (Å²)	SOF
Na	0	0	0	1.08(3)	0.836(6)
S	0.3066(3)	0	0.9329(5)	1.08(3)	1
Fe1	0	0	0.5	1.08(3)	0.856(5)
Fe2	0.75	0.25	0.5	1.08(3)	1
O1	0.4091(6)	0	0.198(1)	1.13(7)	1
O2	0.1679(7)	0	0.829(1)	1.13(7)	1
O3	0.3423(4)	0.1656(6)	0.8460(8)	1.13(7)	1
O4	0.2603(7)	0	0.400(1)	1.13(7)	1
O5	0.0743(4)	0.2023(6)	0.3943(8)	1.13(7)	1

Note: Space group = $C2/m$; unit-cell parameters: a = 12.74852(6), b = 7.34697(3), c = 6.98243(4) Å, β = 127.1974(4)°; R_{wp} = 1.46, χ^2 = 1.035.
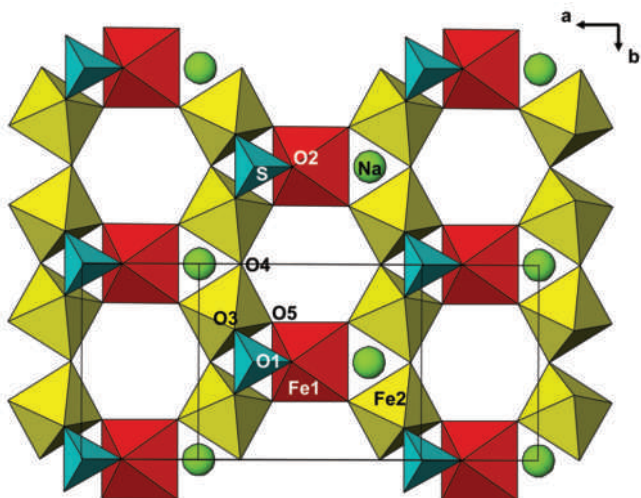
FIGURE 2. A slice along (001) of the monoclinic Na-jarosite structure. Unit cell is shown. Atom labels correspond to Table 1. The Na atoms are shown as filled circles.
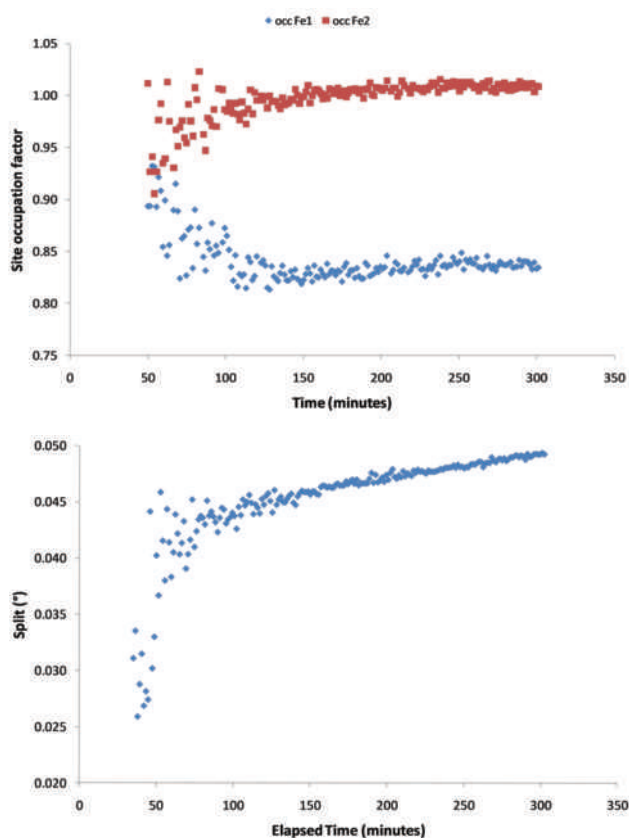

FIGURE 3. Results from Rietveld refinement of in situ synchrotron data sets collected during Na-jarosite synthesis at 95 °C, showing the variation with reaction time of. (**a**) Site occupancy for Fe1 and Fe2 sites. (**b**) Separation between split peaks corresponding to $(012)_h$.

development of ordering of the iron-site vacancies is associated with an increase in the magnitude of the monoclinic distortion. This is illustrated in Figure 3b, showing an increase with time of the splitting of the pair of peaks corresponding to $(012)_h$. A

previous study (Göttlicher et al. 2000), which included a single-crystal refinement of monoclinic K-jarosite, did not detect any variation in iron-site occupancies from the random distribution that applies in the rhombohedral jarosites. A possible explanation is that the crystal used was twinned by rotation around the pseudo-threefold axis. Twinning does not affect the refinement of powder diffraction data.

The results of this study may find application in helping to interpret the magnetic properties of synthetic jarosites. Published magnetic studies frequently comment on the variability of results for synthetic jarosites, and they attribute the variability to the extreme sensitivity of the magnetic properties toward the coverage of the magnetic lattice (Wills et al. 2000; Grohol et al. 2003; Frunzke et al. 2001; Earle et al. 1999; Nielson et al. 2008). Different researchers have consistently found that synthetic iron-deficient jarosites undergo two successive magnetic phase transitions at temperatures in the range 40 to 65 K (Wills et al. 2000; Frunzke et al. 2001; Maegawa et al. 1996). The lowest temperature phase has the classic planar (001) triangular array of spins characteristic of a kagomé lattice, whereas the intermediate temperature phase is reported to have a component of the spins directed along the hexagonal cell c_h axis (Frunzke et al. 2001). One approach to minimize this influence of the variable occupation of the iron sites has been to develop new synthesis methods for the preparation of stoichiometric jarosites (Grohol et al. 2003; Bartlett and Nocera 2005). Although successful, this approach does not address the unusual magnetic effects measured on non-stoichiometric jarosites.

A consideration of the differences between the structures of rhombohedral and monoclinic jarosites provides some insight into such magnetic phenomena. In rhombohedral jarosites, the octahedrally coordinated iron atoms are connected by corner-sharing into chains along three equivalent directions separated by 120° in (001) layers. These intersecting chains form a kagomé net of iron atoms. In monoclinic iron-deficient jarosites, the Fe1 site vacancies are confined to only two of the chains, oriented along [110] and [1$\bar{1}$0] as shown in Figure 2. The third chain, oriented along [010], is fully occupied by Fe2 atoms. Thus locally the (001) layers comprise only [010] chains of iron-centered octahedra. If the Fe1 vacancies are concentrated in domains, then it is evident that triangular spin frustration cannot occur in these domains. The local magnetic interactions will correspond to those controlled by superexchange along the [010] chains of corner-connected Fe2-centered octahedra. The two reported magnetic transition temperatures in some synthetic iron-deficient jarosites may be due to a combination of regions of ordered and disordered iron vacancies.

This study has shown that iron-deficient jarosites can be synthesized with either complete disorder of the iron-site vacancies (rhombohedral K-jarosite prepared at 95 °C) or with ordering of the iron-site vacancies (monoclinic Na-jarosite, 95 °C). Comparative magnetic studies are warranted on carefully characterized monoclinic vs. rhombohedral jarosites to determine the influence of iron-site vacancy ordering on the magnetic properties.

REFERENCES CITED

Bartlett, B.M. and Nocera, D.G. (2005) Long-range magnetic ordering in iron jarosites prepared by redox-based hydrothermal methods. Journal of the American Chemical Society, 127, 8985–8993.

Basciano, L.C. and Peterson, R.C. (2007) Jarosite-hydronium jarosite solid-solution series with full iron site occupancy: Mineralogy and crystal chemistry. American Mineralogist, 92, 1464–1473.

——— (2008) Crystal chemistry of the natrojarosite-jarosite and natrojarosite-hydronium jarosite solid-solution series: A synthetic study with full Fe site occupancy. American Mineralogist, 93, 853–862.

Bruker (2008) TOPAS Version 4.1. Bruker AXS, Karlsruhe, Germany.

Dutrizac, J.E. (1983) Factors affecting alkali jarosite precipitation. Metallurgical Transactions B, 14B, 531–539.

Dutrizac, J.E. and Jambor, J.L. (2000) Jarosites and their applications in hydrometallurgy. In C.N. Alpers, J.L. Jambor, and D.K. Nordstrom, Eds., Sulfate minerals: Crystallography, geochemistry, and environmental significance, 40, p. 405–443. Reviews in Mineralogy and Geochemistry, Mineralogical Society of America, Chantilly, Virginia.

Earle, S.A., Ramirez, A.P., and Cava, R.J. (1999) The effect of gallium substitution for iron on the magnetic properties of hydronium iron jarosite. Physica B, 262, 199–204.

Frunzke, J., Hansen, T., Harrison, A., Lord, J.S., Oakley, G.S., Visser, D., and Wills, A.S. (2001) Magnetic ordering in diluted kagomé antiferromagnets. Journal of Materials Chemistry, 11, 179–185.

Göttlicher, J., Gasharova, B., and Bernotat-Wulf, H. (2000) Pseudotrigonal jarosites $(K,H_3O)Fe_3(SO_4)_2(OH)_6$. Geological Society of America, Abstracts with programs, 32, A180.

Grohol, D., Nocera, D.G., and Papoutsakis, D. (2003) Magnetism of pure iron jarosites. Physical Review B, 67, 064401.

Jones, E.J.P., Nadeau, T.-L., Voytek, M.A., and Landa, E.R. (2006) Role of microbial iron reduction in the dissolution of iron hydroxysulfate minerals. Journal of Geophysical Research, 111, G01012.

Klingelhöfer, G., Morris, R.V., Bernhardt, B., Shröder, C., Rodinov, D.S., de Souza, P.A., Yen, A., Gellert, R., Evlanov, E.N., Zubkov, B., and others (2004) Jarosite and hematite at Meridiani Planum from Opportunity's Mössbauer spectrometer. Science, 306, 1740–1745.

Kolitsch, U. and Pring, A. (2001) Crystal chemistry of the crandallite, beudantite and alunite groups: a review and evaluation of the suitability as storage materials for toxic metals. Journal of Mineralogical and Petrological Sciences, 96, 67–78.

Madsen, I.C., Scarlett, N.V.Y., and Whittington, B.I. (2005) Pressure acid leaching of nickel laterite ores: an in situ diffraction study of the mechanism and rate of reaction. Journal of Applied Crystallography, 38, 927–933.

Maegawa, S., Nishiyama, M., Tanaka, N., Oyamada, A., and Takanao, M. (1996) Observation of successive phase transitions in kagomé lattice antiferromagnets $RFe_3(OH)_6(SO_4)_2$ [R = NH$_4$, Na, K]. Journal of the Physical Society of Japan, 65, 2776–2778.

Nielson, U.G., Majzlan, J., and Grey, C.P. (2008) Determination and quantification of the local environments in stoichiometric and defect jarosite by solid-state ^{2}H NMR spectroscopy. Chemistry of Materials, 20, 2234–2241.

Papike, J.J., Karner, J.M., and Shearer, C.K. (2006) Comparative planetary mineralogy: Implications of Martian and terrestrial jarosite. A crystal chemical perspective. Geochimica et Cosmochimica Acta, 70, 1309–1321.

Wills, A.S., Harrison, A., Ritter, C., and Smith, R.I. (2000) Magnetic properties of pure and diamagnetically doped jarosites: Model kagomé antiferromagnets with variable coverage of the magnetic lattice. Physical Review B, 61, 6156–6169.